

Modeling and Simulation of the Influence of Dielectric Cavity on the HVDC Transmission Cable

F. HASSAINE^a, H. NOURI^{a,*}, H. AIT SAID^b,
K. MEZIANE^c AND M. AISSOU^d

^a*Department of Electrical Engineering, Ferhat Abbas University, Setif 19000, Algeria*

^b*Electrical Engineering and Automatic Department, University of Relizane, Relizane 48000, Algeria*

^c*Electrical Engineering Department, University of Khemis Miliana, Khemis Miliana 44000, Algeria*

^d*Electrical Engineering Department, University of Ain Temouchent, Ain Temouchent 46000, Algeria*

Received: 06.09.2024 & Accepted: 02.12.2024

Doi: [10.12693/APhysPolA.147.116](https://doi.org/10.12693/APhysPolA.147.116)

*e-mail: nouri_hamou@yahoo.fr

Partial discharge is one such phenomenon that can be monitored to assess the quality of insulation. However, this phenomenon is quite intricate and requires an understanding of various concurrent processes. This paper aims to analyze the behavior of the cable for the transport of direct current at high voltage. At the fundamental level, partial discharge is a localized breakdown that occurs without complete bridging of the insulation. The essential electrical properties that influence the optimal operation of high-voltage direct current cables are studied and analyzed numerically. The distribution of potential and electric field are determined by solving the Poisson equation using the finite difference method. The results of the numerical simulation for the different parts of the cable in the presence of partial discharges are presented and interpreted. Some aspects of this effect require further investigations in order to validate a realistic mathematical model of the physical phenomena as an essential step towards the accurate numerical simulation of the cable life approximation process.

topics: power transmission cable, high-voltage direct current (HVDC), partial discharge, Maxwell's equations

1. Introduction

Currently, a large number of high-voltage lines in the world are powered by three-phase alternating current. But, in the particular context of some submarine crossings or buried lines, transport is done using high-voltage direct current (HVDC) for reasons of economy, size, reliability, and availability. Its main purpose is to allow the transport of electricity over long distances, which generates fewer losses. The power-carrying capacity of an alternating current (AC) line is inversely proportional to the transmission distance. The power-carrying capacity of direct current (DC) lines is not affected by the transmission distance. HVDC is the optimal solution for transporting electricity in buried or underwater cables over distances greater than approximately 100 km. In fact, the reactive power produced by the capacitive nature of the cable powered by alternating current ends up preventing the transport of the sought active power. In direct current, no reactive power is produced in the cable [1–5].

The cost of a transmission line includes the capital investment required for the actual infrastructure and the costs incurred for operational needs. The direct current line can carry as much power with two conductors (having positive/negative polarities with respect to ground) as an alternating current line with three conductors of the same size. Therefore, for a given power level, a DC line requires a small line, simpler and cheaper pylons, and reduced conductor and insulation costs. DC lines do not require reactive power compensation. However, terminal equipment costs are increased due to the presence of converters and filters.

The use of HVDC allows for the reduction of power transmission losses to approximately two-thirds of those of the high-voltage alternating current (HVAC) system. The absence of skin effect in DC is also beneficial in marginally reducing power losses, and the dielectric losses in the case of power cables are also much lower for DC transmission. The effects of corona discharge tend to be less significant for direct current conductors than for alternating current conductors.

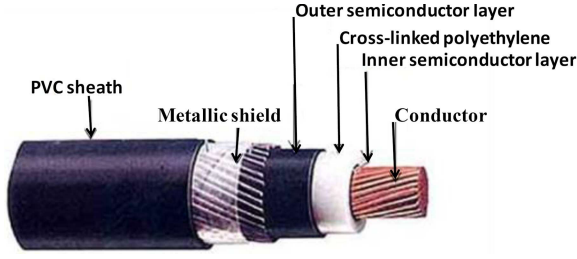


Fig. 1. Design of a polymer-insulated cable.

Due to its rapid controllability, DC transmission has full control over the transmitted power and the ability to improve transient and dynamic stability in associated AC networks. It can also limit fault currents in direct current lines. Additionally, direct current transmission overcomes some of the problems associated with alternating current transmission.

Therefore, planning DC transmission for various technological applications requires a detailed study to assess the benefits. Currently, the number of direct current lines in an electrical network is very small compared to the number of alternating current lines. This indicates that DC transmission is only justified for specific applications, although technological advancements and the introduction of multi-terminal DC systems are expected to increase DC lines.

Cables used in direct current connections are subject to constant electrical stress and therefore must be designed differently from those used in alternating current. Due to the constant electrical stress subjected to the insulation of the cables, the presence of partial discharges in the insulation modifies the distribution of the internal electric field, inducing significant local reinforcements of the electric field, which will lead to a strong distortion of the theoretical field, which can lead to an acceleration of the aging of the cable [6–11]. The aging of the insulation generally leads to an increase in structural defects, likely to trap charges and overheat the different layers of the cable. The simultaneous presence of electrical and thermal gradients applied to the cable insulation leads to a redistribution of the electric field in the insulation, moving from capacitive behavior to resistive behavior. For a resistive distribution of the electric field, the resistivity of the insulator strongly depends on both the electric field and the temperature. The presence of space charges in the insulation of high-voltage cables poses a real reliability problem. Until now, no method has allowed for a direct measurement and localization of these charges in a cable with thick insulation [12].

Currently, the most widely used material for HVDC cable insulation is low-density polyethylene. To reduce its conductivity, additives, such as high-density polyethylene, metal oxide nanoparticles, carbon allotropes, or various aromatic molecules,

are added to the plastic. These additives trap electrical charges and reduce their mobility, which helps reduce electrical conductivity.

2. Problem description

Figure 1 shows the geometry of our problem. The simulation model is deduced from the real case, which is a coaxial wire–cylinder configuration that presents perfect symmetry of revolution; moreover the electrodes are considered to have infinite length along the wire.

Section of a 90 kV extruded electric cable model is characterized by the copper conductor in the center surrounded by polymer insulation, i.e., cross-linked polyethylene, followed by a semiconductor layer, a few copper conductors, an aluminum sheath, and finally a plastic protection.

2.1. Mathematical model

The basic equations governing the phenomenon of partial discharges in electrical energy transmission cables are reduced to Maxwell's equations of electrostatics to which are added the equations of the considered environment. These equations are [13–18]

$$\nabla \cdot \mathbf{E} = \pm \frac{\rho}{\varepsilon_0 \varepsilon_r}, \quad (1)$$

$$\nabla \cdot \mathbf{J} = 0, \quad (2)$$

$$\mathbf{J} = \pm \rho \mu \mathbf{E}, \quad (3)$$

$$\mathbf{E} = -\nabla U, \quad (4)$$

$$\nabla^2 U = \mp \frac{\rho}{\varepsilon_0 \varepsilon_r}, \quad (5)$$

where

- \mathbf{E} is the electric field vector [V/m]. The sign in (1) is positive if the active electrode is subjected to a voltage of positive polarity, and negative otherwise;
- U is the electric potential [V];
- ρ is the space charge density [C/m³] and is always positive. The sign in (5) is negative if the active electrode is subjected to a voltage of positive polarity, and positive otherwise;
- \mathbf{J} is the current density vector [A/m²]. The sign in (3) is positive if the applied voltage is of positive polarity, and negative otherwise;
- μ is the mobility of positive or negative ions depending on the polarity of the active electrode [m²/(V s)];
- ε_0 is the absolute permittivity of vacuum ($\varepsilon_0 = 8.85 \times 10^{-12}$ F/m);
- ε_r is the relative permittivity of the material considered.

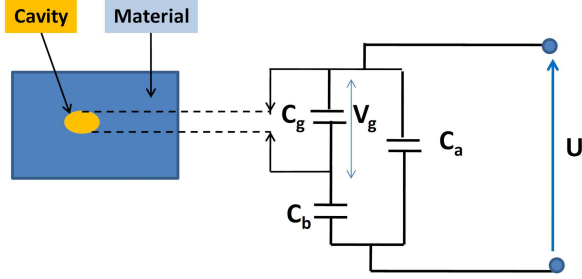


Fig. 2. Partial discharge simulation model.

Equation (5) is the Poisson equation; it is obtained by replacing the field expression given by (2) in (1). Equation (2) is the current continuity equation. Equation (3) is the current density equation.

In reality, it is extremely difficult to find an exact solution to these equations due to their non-linear nature, and thus, simplifying approaches based on hypothetical models are introduced to find solutions to real problems. Several simplifying hypotheses were introduced to solve the problem. Therefore, a numerical solution is provided as a tool for solving this set of equations [19–23].

2.2. Modeling a dielectric insulation with the cavity

The breakdown mechanisms in polymer (PE) can be divided into electric, thermal, electromechanical, and partial discharge mechanisms [24].

Partial discharges occurring in gas-filled voids degrade the insulation and, under certain circumstances, can initiate electrical trees. The electrical trees can continue propagating through the insulation by continued discharges and finally give rise to breakdown.

Causes of partial discharges are local increases in field strength (for example, at conductive points or through field displacement) or local reductions in electric strength (e.g., due to gas-filled cavities). The inception field strength for streamer discharges in cavities is given by [25, 26]

$$E_C = 25.2 U_p \left(1 + \frac{8.6}{\sqrt{pd}} \right). \quad (6)$$

The limiting voltage for the appearance of discharges on the dielectric is given by

$$V_C = e E_C \left[1 + \frac{1}{\varepsilon_r} \left(\frac{d}{e} - 1 \right) \right]. \quad (7)$$

The electrical modeling of a partial discharge in a cavity within an insulator can be translated using an equivalent capacity diagram. The cavity can be modeled by the capacitance, the part of the dielectric surrounding the cavity by the capacitance C_b in series with C_g , and the flawless part of the dielectric

will be represented by the capacitance C_a , parallel to the other branch. Such a scheme is presented in Fig. 2, where

- C_g — capacitance of the cavity, which is parallel to the C_a spark gap. When the cavity breakdown voltage is reached, the spark gap shorts out;
- C_b — capacitance of the dielectric without partial discharge in series with the cavity;
- C_a — equivalent capacitance of the insulation in parallel with C_g and C_b . This capacity corresponds to the sound part of the insulation;
- U — voltage applied to the terminals of the dielectric;
- V_g — the voltage across the cavity;
- e — cavity thickness;
- d — dielectric thickness;

and where

$$C_g = \varepsilon_0 \frac{S}{e}, \quad (8)$$

$$C_b = \varepsilon_0 \varepsilon_r \frac{S}{d - e}, \quad (9)$$

$$V_g = U \frac{C_b}{C_b + C_g}. \quad (10)$$

When air gap capacitance C_g voltage at both ends reaches discharge voltage V_0 , a partial spark discharge occurs in the air gap V_g . When V_g drops to extinction, the spark is extinguished, a partial discharge is completed, and a high-frequency partial discharge pulse current is generated in the circuit [27].

This void will become the source of a partial discharge if the applied voltage is increased, as the field gradients in the void are strongly enhanced by the difference in permittivities as well as by the shape of the cavity [28].

2.3. Boundary conditions

As a boundary condition, Townsend assumed that the electric field on the active electrode remains constant and is everywhere equal to the threshold value. Kaptzov postulated that the field distribution on the surface of the crowned conductor remains constant and is equal to its threshold value even if the applied voltage increases.

Near the surface of the high-voltage conductor, the applied voltage is $U = 90$ kV and

$$E = E_{Peek} = 32.3 \times 10^5 \delta + 0.846 \times 10^5 \sqrt{\delta/R_1}, \quad (11)$$

$$\rho_0 = \frac{Q_0}{V_1} = \frac{Q_0}{\pi R_1^2 l}, \quad (12)$$

where Q_0 is the total charge of the cable in the absence of charges in the dielectrics and semiconductors; R_1 is the radius of copper conductive core; l is the cable length = 50 m; δ is the relative density of air.

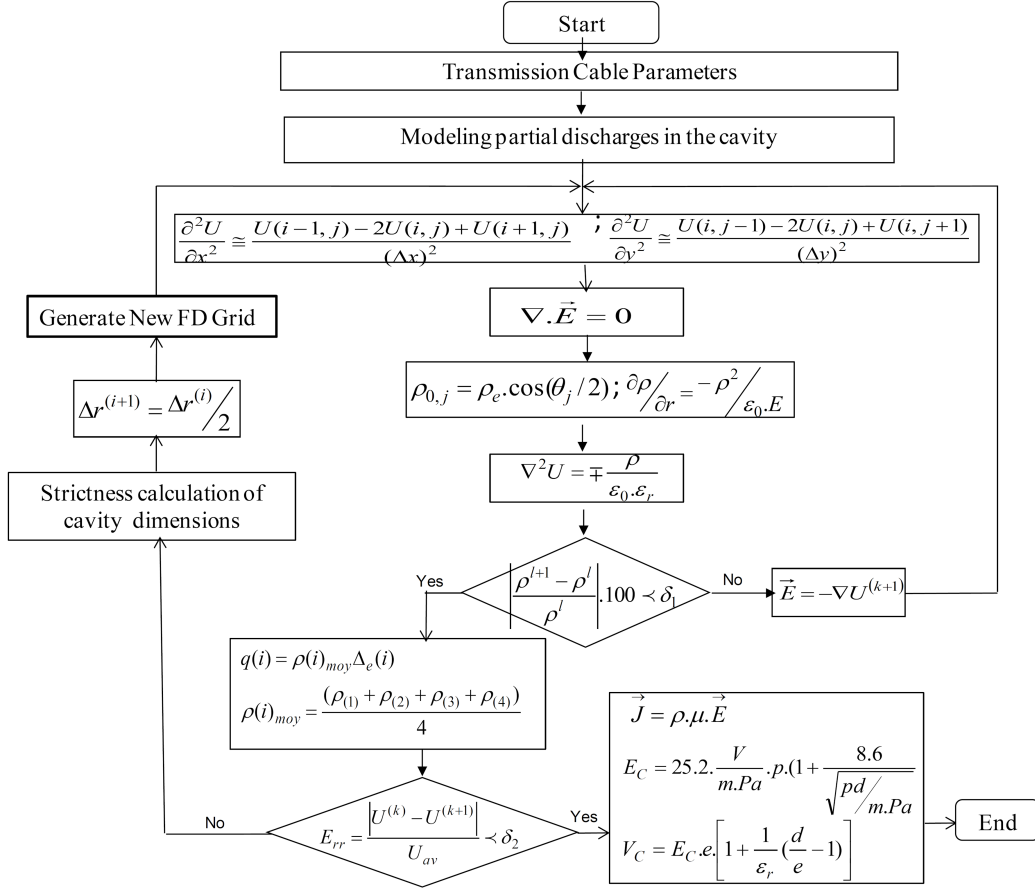


Fig. 3. Flowchart for solving the corona discharge problem in a wire-cylinder configuration.

To avoid the effect of the ends, we assume that the length of the cable is infinite ($l \gg R_1$).

2.4. Method for solving the Poisson equation

To go from a continuous exact problem governed by a partial differential equation to a discrete approximate problem, we used the finite difference method. The method consists in replacing partial derivatives by divided differences or combinations of point values of a characteristic function. Solving an equation by the finite difference method amounts to replacing the search for a continuous solution with the solution at a certain number of points [29, 30]. Any distribution of points in space can be used. It consists in decomposing the study area into a uniform rectangular grid, in which each node is equidistant from its neighbor along the x and y axes, and at each node, the differential system is satisfied.

The finite difference method uses a mesh with constant steps (regardless of the type of coordinates used) and offers two types of solutions. The first is explicit, i.e., the unknowns at the nodes of the mesh are given explicitly by the equations. The second

type is implicit, i.e., the unknowns constitute a linear system that must be inverted and is based on a “hollow” matrix form. Therefore, we can approximate the operators of a differential equation by finite differences calculated at the nodes of a mesh. Also, we can approximate the unknown function of a differential equation.

In the first step of the resolution, we replace the derivatives of order 2 in (5) with the following expressions

$$\frac{\partial^2 U}{\partial x^2} \cong \frac{U(i-1, j) - 2U(i, j) + U(i+1, j)}{(\Delta x)^2}, \quad (13)$$

$$\frac{\partial^2 U}{\partial y^2} \cong \frac{U(i, j-1) - 2U(i, j) + U(i, j+1)}{(\Delta y)^2}. \quad (14)$$

So, we find the unknown function with two variables

$$\nabla^2 U = \frac{\partial^2 U}{\partial x^2} + \frac{\partial^2 U}{\partial y^2} = \mp \frac{\rho}{\epsilon_0 \epsilon_r} \Rightarrow U(i, j) = \frac{U(i-1, j) + U(i+1, j) + U(i, j-1) + U(i, j+1) + h^2}{4}. \quad (15)$$

The partial differential equation is then replaced by a system of algebraic equations for the nodal values. We end up with a linear system in matrix form

$$AU = B, \quad (16)$$

Characteristics of the cable used in the simulation.

TABLE I

Element	Type	Thickness [mm]	Relative permittivity	Resistivity [Ω m] at 20°C
conductor	Al	7	8.00	2.65×10^{-8}
inner semiconductor layer	Si	1	11.68	2.2×10^3
insulation	XLPE	10	2.50	3.2×10^{11}
outer semiconductor layer	GaAs	1	12,40	5×10^{-6}
metallic shield	Cu	2	0.99	1.68×10^{-8}
jacket: outer sheath	PVC	3.5	5.00	10^{11}

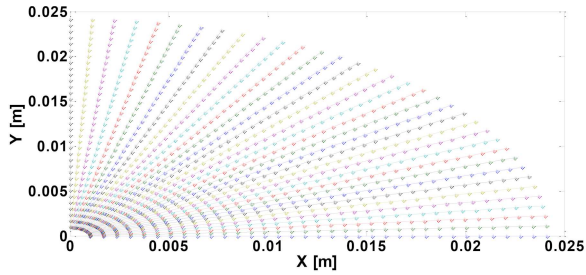


Fig. 4. Field lines for $\frac{1}{4}$ of the calculation domain.

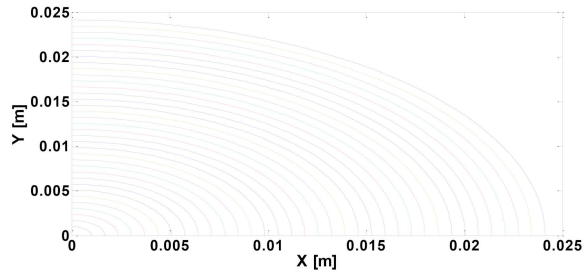


Fig. 5. Equipotential contours for $\frac{1}{4}$ of the calculation domain.

where A is the stiffness matrix; U is the matrix of potentials at the nodes; B is the second member of the system.

After solving linear system (16), we find the first solution which represents the distribution of the potential in the calculation domain.

The flowchart for solving the considered problem is given in Fig. 3. The different steps followed for the numerical resolution are detailed in Sect. 3.

3. Results and discussions

In this investigation, we reported the results obtained by applying the proposed flowchart to the cylindrical configuration. The accuracy of our method depends on the accuracy of the model parameters. However, there are other parameters that play an important role in the accuracy and speed of calculations.

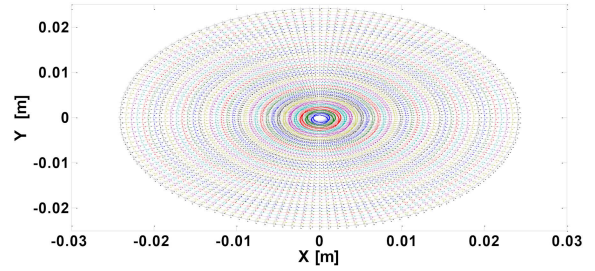


Fig. 6. Rectangular mesh of the cable geometric model.

The HVDC cable studied has the characteristics given in Table I. The active electrode is subjected to a direct voltage of 110 kV. The cable is 25 m long. The material chosen as insulation is cross-linked polyethylene (XLPE). The metal screen is grounded.

3.1. Discretization domain

The use of a regular mesh makes it possible to have, at every point, the same form for the equations. The simplest of the regular meshes is the square mesh (see Figs. 4–6).

The calculation is extended to a set of the calculation domain, which is subdivided into small elements by rectangular mesh, where each rectangle is identified by its four vertices (nodes).

The mesh presented in Fig. 6 is the mesh that we chose to discretize our calculation domain. It is generated from equipotential and field lines.

To achieve a compromise between precision and the time necessary to draw Fig. 6, the increment is chosen to be constant to obtain a uniform mesh. The node (i, j) is given by the intersection of the i -th line with the j -th contour.

A field figure is, by definition, a curve tangent at each point to the field vector defined at that point. We also note that the field lines do not intersect. They carry positive charges towards negative charges (or to infinity).

3.2. Electric potential

The potential function defines a field of scalars, which describes the electrical properties of space. The set of points in space that are at the same potential constitutes an equipotential surface. The distribution of the electric potential between two electrodes is shown in Figs. 7–8.

3.3. Electric field

Having estimated all the potential values at the nodes of the mesh, the estimation of the electric field values is carried out by the interpolation/extrapolation method.

Given a distribution of charges is considered external, it is therefore always possible to define at each point \mathbf{r} in space a vector quantity $\mathbf{E}(\mathbf{r})$ called the electric field. The distribution of the electric field in our system is shown in Figs. 9–10.

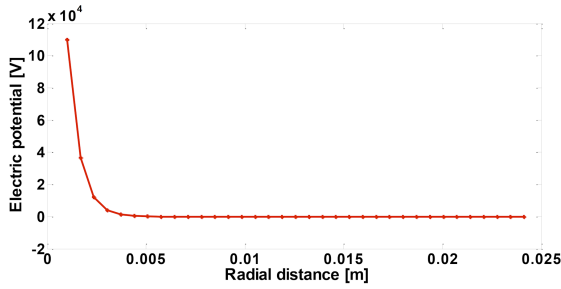


Fig. 7. Variation of electric potential.

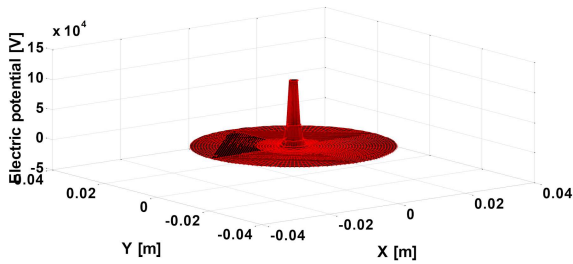


Fig. 8. Distribution of electric potential between two electrodes.

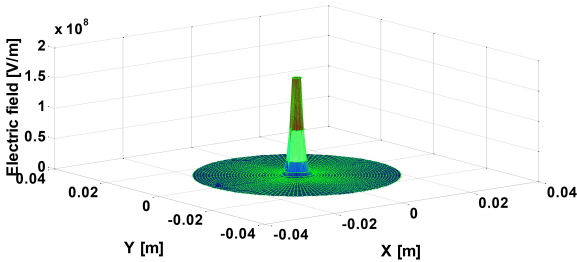


Fig. 9. Electric field distribution between two electrodes.

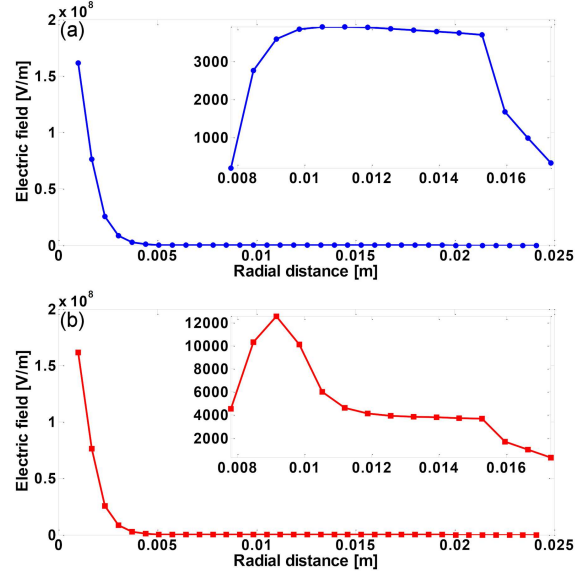


Fig. 10. Variation of the electric field: (a) in the absence of a cavity, (b) in the presence of a cavity.

Knowing an electric field E means knowing the electric field vector at each point in space, in direction and intensity. In some simple cases, it is given by an algebraic relation. In more complex cases, it can be calculated at sufficiently fine mesh points.

With current computer resources, it is very easy to write a program such that, after entering the loads and their positions, the computer provides at each requested point M a small arrow whose direction and length provide information on the electric field at this point.

From the field variations between the two electrodes, we can notice a flattening in the direction of the collector plane because of the high ratio between the electric field on the wire and that of the ground plane.

Data from the potential and electric field distributions will be used to re-estimate the space charge density at the nodes. This procedure continues until the error on the potential becomes less than a predetermined value. The error is defined by

$$E_{rr} = \frac{|U^{(k)} - U^{(k+1)}|}{U_{av}}, \quad (17)$$

$$U_{av} = \frac{(U^{(k)} + U^{(k+1)})}{2}, \quad (18)$$

where k is the iteration number.

Once the error has been estimated, it is possible to control the quality of the solution by calculating the optimal size of each element of the mesh. This amounts to constructing an optimal mesh, either in the sense of imposed precision or in the sense of the maximum size of the problem studied. This involves developing a mesh adaptation strategy.

3.4. Space charge density

The electric charge is the source of the electric field, so the electric field at any point in space can be mathematically related to the charges present.

The benefit of space charge density is shown in Figs. 11–12.

This step is necessary for the resolution of the Poisson equation by the finite difference method, the execution procedure of which is given in the following steps. However, we introduced a third boundary condition of the potential corresponding to the critical field of the ionization minimum.

3.5. Current density

Figure 13 gives the variations of the current density as a function of the applied voltage and the interelectrode distance inside the system.

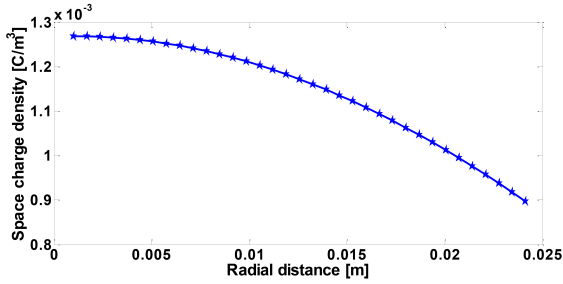


Fig. 11. Variation of the space charge density between two electrodes without dielectric.

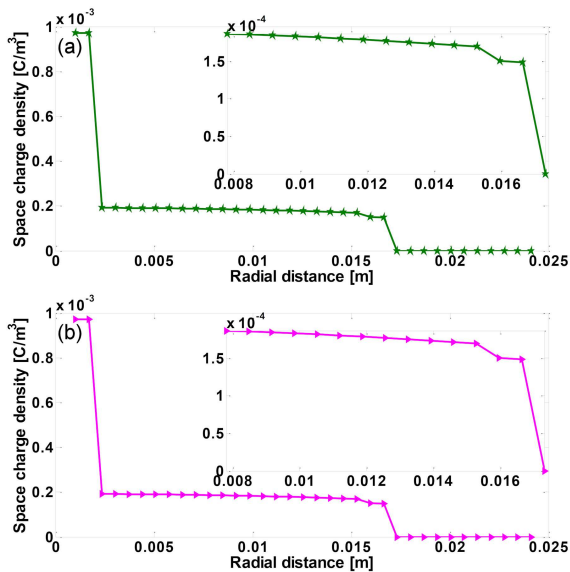


Fig. 12. Variation of the space charge density in the cable: (a) in the absence of a cavity, (b) in the presence of a cavity.

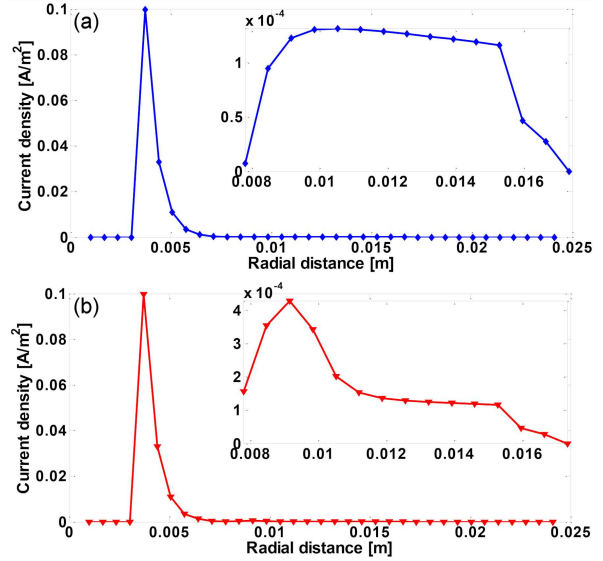


Fig. 13. Variation of electric current density in the interelectrode space: (a) in the absence of a cavity, (b) in the presence of a cavity.

This variation is in good agreement with Townsend’s theoretical current–voltage law. We see that if the distance increases, the current density decreases.

4. Conclusions

In this work, a numerical technique for simulating the electric properties of HVDC cable has been presented. The ionized field of a unipolar DC cable is modeled as the ionized field of a single cylindrical conductor with the presence of partial discharge in the dielectric. The discharge is described by the equation for the density of positive ions of a single species and Poisson’s equation for the electric field.

The finite difference method used for the resolution of the problem presents a good approximation in the determination of the electrical characteristics of the HVDC power transmission cable coupled to the partial discharges. Very high-voltage cables are increasingly used to transport electricity over long distances. However, the more the voltage increases, the less efficient the insulation of the cables becomes.

This electrical study is very useful for analyzing the condition of the cable in service. If the potential difference across the cavity is less than the breakdown voltage, the cable remains in service. Otherwise, it is recommended to change the cable to ensure the proper functioning of the electrical installations. The technique used in practice is to gradually increase the voltage across the sample up to the limit voltage, which corresponds in

the cavity to the breakdown field of the gas. As a result of the dissipation of energy in the cavity, there is neutralization of charge on the walls of the latter.

References

- [1] M.H. Rashid, *Power Electronics Handbook* 4th ed., Elsevier, Butterworth-Heinemann, 2018, p. 575.
- [2] H. Ghorbani, M. Jeroense, C.-O. Olsson, M. Saltzer, *IEEE Trans. Power Deliv.* **29**, 414 (2014).
- [3] Y. Späck-Leigsnering, G. Ruppert, E. Gjonaj, H. De Gersem, M. Koch, *Energies* **14**, 2848 (2021).
- [4] S.J. Frobin, C.F. Niedik, C. Freye, F. Jenau, D. Häring, G. Schröder, in: *2018 IEEE 2nd Int. Conf. on dielectrics (ICD)*, 2018.
- [5] H. Nouri, A. Tabbel, N. Douib, H. Aitsaid, Y. Zebboudj, *Int. J. Electr. Comput. Eng.* **9**, 627 (2015).
- [6] A.S. Bhangaonkar, S.V. Kulkarni, in: *2008 IEEE Int. Power Modulators and High-Voltage Conf.*, 2008, p. 572.
- [7] J. Wang, R. Guo, A. Ping, T. Liu, S. Han, Q. Li, *High Volt.* **7**, 439 (2022).
- [8] E. Ouatah, S. Megherfi, K. Haroun, Y. Zebboudj, *Electr. Power Syst. Res.* **99**, 38 (2013).
- [9] J.M. Rodríguez-Serna, R. Albarracín-Sánchez, A.A. Mas'ud, *High Volt.* **5**, 556 (2020).
- [10] N. Oussalah, Y. Zebboudj, S.A. Boggs, *IEEE Trans. Dielectr. Electr. Insul.* **14**, 1264 (2007).
- [11] D. Pommerenke, R. Jobava, R. Heinrich, *IEEE Electr. Insul. Mag.* **18**, 6 (2002).
- [12] A. Toureille, J.-P. Reboul, P. Merle, *Phys. III France* **1**, 111 (1991).
- [13] H. Nouri, H. Ait Said, Y. Zebboudj, N. Zouzou, L. Dascalescu, *IEEE Trans. Dielectr. Electr. Insul.* **23**, 665 (2016).
- [14] H. Nouri, M. Aissou, H. Ait Said, Y. Zebboudj, *Int. J. Numer. Modell.* **28**, 138 (2015).
- [15] L.M. Dumitran, L. Dascalescu, P. Nothinger, P. Atten, *J. Electrostat.* **65**, 758 (2007).
- [16] M.S. Mokrov, Y.P. Raizer, *Plasma Phys. Rep.* **47**, 568 (2021).
- [17] K. Adamiak, P. Atten, *J. Electrostat.* **61**, 85 (2004).
- [18] H. Nouri, Y. Zebboudj, *Eur. Phys. J. Appl. Phys.* **49**, 11001 (2010).
- [19] W. Deutsh, *Ann. Phys.* **373**, 335 (1922).
- [20] N.A. Kaptzov, *Elektricheskie Invlentia v Gazakh i Vakuumme*, OGIZ, Moscow 1947, p. 587.
- [21] V.I. Popkov, *Elektrichestvo* **1**, 33 (1949).
- [22] M.P. Sarma, W. Janischewskyj, *IEEE Trans. Power App. System* **88**, 718 (1969).
- [23] J.M. Townsend, *Electricity in Gases*, Oxford University Press, 1914.
- [24] L.A. Dissado, J.C. Fothergill, *IEEE Materials and Devices Series 9*, Peter Peregrinus, London 1992.
- [25] A. Küchler, *High Voltage Engineering, Fundamentals — Technology — Applications*, 1st ed., VDI-Buch, Springer-Verlag, Berlin 2018 p. 249.
- [26] F. Gutfleisch, L. Niemeyer, *IEEE Trans. Dielectr. Electr. Insul.* **2**, 729 (1995).
- [27] J. Sun, S. Pan, J. Deng, *J. Phys. Conf. Ser.* **2195**, 012024 (2022).
- [28] E. Kuffel, W.S. Zaengl, J. Kuffel, *High Voltage Engineering Fundamentals*, 2nd ed., Butterworth-Heinemann, 2000 p. 395.
- [29] A. Bossavit, C. Emson, D. Mayergoyz, *Méthodes Numériques en Électromagnétisme*, Eyrolles, Paris 1991.
- [30] H.J. Lee, W.E. Schiesser, *Ordinary and Partial Differential Equation Routines in C, C++, Fortran, Java, Maple and Matlab*, Chapman & Hall/CRC Press Company, 2004, p. 20.